

Magnetic field dependence of nucleon parameters from QCD sum rules

C. A. Dominguez¹, Luis A. Hernández^{1,2,3}, Marcelo Loewe^{4,5,1}, Cristian Villavicencio^{6,*} and R. Zamora^{7,8}

¹*Centre for Theoretical & Mathematical Physics, and Department of Physics,
University of Cape Town, Rondebosch 7700, South Africa;*

²*Instituto de Ciencias Nucleares, Universidad Nacional Autónoma de México, Apartado Postal 70-543, CdMx 04510, Mexico;*

³*Facultad de Ciencias de la Educación, Universidad Autónoma de Tlaxcala, Tlaxcala, 90000, Mexico;*

⁴*Instituto de Física, Pontificia Universidad Católica de Chile, Casilla 306, Santiago, Chile;*

⁵*Centro Científico Tecnológico de Valparaíso-CCTVAL,
Universidad Técnica Federico Santa María, Casilla 110-V, Valparaíso, Chile;*

⁶*Centro de Ciencias Exactas & Departamento de Ciencias Básicas,
Facultad de Ciencias, Universidad del Bío-Bío, Casilla 447, Chillán, Chile;*

⁷*Instituto de Ciencias Básicas, Universidad Diego Portales, Casilla 298-V, Santiago, Chile; and*

⁸*Centro de Investigación y Desarrollo en Ciencias Aeroespaciales (CIDCA), Fuerza Aérea de Chile, Santiago, Chile.*

Finite energy QCD sum rules involving nucleon current correlators are used to determine several QCD and hadronic parameters in the presence of an external, uniform, large magnetic field. The continuum hadronic threshold s_0 , nucleon mass m_N , current-nucleon coupling λ_N , transverse velocity v_\perp , the spin polarization condensate $\langle \bar{q}\sigma_{12}q \rangle$, and the magnetic susceptibility of the quark condensate χ_q , are obtained for the case of protons and neutrons. Due to the magnetic field, and charge asymmetry of light quarks *up* and *down*, all the obtained quantities evolve differently with the magnetic field, for each nucleon or quark flavor. With this approach it is possible to obtain the evolution of the above parameters up to a magnetic field strength $eB < 1.4 \text{ GeV}^2$.

PACS numbers: 12.38.Aw, 12.38.Lg, 12.38.Mh, 25.75.Nq

I. INTRODUCTION

The influence of external, strong magnetic fields on hadronic and Quantum Chromodynamics (QCD) properties is an active research field. There are two important physical scenarios involving these extreme magnetic fields, i.e. peripheral heavy ion collisions, and compact stars such as magnetars. Several methods have been employed in order to extract the magnetic evolution of various quantities, e.g. masses, coupling constants, and QCD vacuum condensates. These are, among others, lattice QCD, linear sigma model, Walecka model, Nambu–Jona-Lasinio model, functional renormalization group, and QCD sum-rules.

Lack of experimental data makes it imperative to explore different perspectives for a better understanding of such systems. There are a few open questions in this field, e.g. the magnetic behavior of vacuum condensates. However, there is a consensus with respect to the existence of magnetic catalysis of the chiral condensate at zero temperature [1]. For this reason, the chiral condensate at finite magnetic field can be considered as a reliable input in several analysis. The magnetic behavior of other condensates, e.g. the gluon condensate, is still not well established. However, there seems to be a reasonable consensus within a certain region of the magnetic field strength [2, 3]. In the case of new condensates appearing in the presence of an external magnetic field, the main object is the polarization tensor condensate $\langle \bar{q}\sigma_{\mu\nu}q \rangle$. All approaches agree on the linear behavior of this object for

weak magnetic fields [1, 4].

The baryon sector, in particular the nucleon case, in magnetic fields has been less explored. As a result, there are several pending issues. For instance, the magnetic behavior of the nucleon mass is unclear. In fact, different approaches lead to different behavior. Some models lead to an increasing mass with increasing field, others lead to the opposite behavior, and still others suggest no significant magnetic field dependence [5–9].

QCD sum rules have been used to study magnetic field effects in baryonic systems. Early work was focused on the determination of the nucleon magnetic moment in the presence of new condensates [10]. This procedure was later extended to the full baryonic octet [11]. These approaches considered only linear magnetic field dependences, and included the new condensate. We consider here Finite Energy QCD sum rules (FESR) in an external magnetic field to obtain the behaviour of various QCD and hadronic parameters. The analysis is not restricted to linear magnetic field dependences. These sum rules allow for the extraction of information about the hadronic continuum threshold s_0 , the current-nucleon coupling λ_N , the transverse velocity of nucleons, the polarization tensor of the condensate, the magnetic susceptibility of the quark condensate, and the nucleon masses. For this purpose, techniques used in previous work are implemented [2, 12, 13].

This paper is organized as follows. In Section II we present a brief introduction to FESR, and their application to the vacuum correlation of nucleonic interpolating currents. Section III is devoted to the introduction of an external magnetic field, specifying in detail the changes in

* E-mail: cvillavicencio@ubiobio.cl

propagators, correlator structures, and the corresponding modifications induced in the FESR. In section IV we present the set of QCD sum rules together with the numerical analysis. The article ends with the conclusions in section V.

II. VACUUM FESR

A. Brief description of FESR

The FESR involve current-current correlators in momentum space $\Pi(p^2)$ multiplied by some analytic kernel (for a review see e.g. [14]). These correlators are integrated along a closed contour consisting of a circular path in the complex plane $s = p^2$, skipping the singularities and branch cut that lie along the real positive s -plane (the *pac-man* contour) [2, 12, 13]. From Cauchy's theorem the contour integral can be expressed as

$$\frac{1}{\pi} \int_0^{s_0} ds K(s) \text{Im} \Pi(s)|_{\text{Had}} = \frac{-1}{2\pi i} \oint_{s_0} ds K(s) \Pi(s)|_{\text{QCD}}, \quad (1)$$

where $K(s)$ is an analytic kernel, usually a power of s , and the integration path on the right hand side is a circle of radius s_0 . This expression encapsulates the notion of quark-hadron duality, with hadronic information along the positive real axis being related to QCD on the circle. One of the advantages of FESR with respect to other sum rules is that they provide a projection of vacuum condensates of a given mass dimension for each power of s .

B. Nucleon FESR

The issue of the correlator involving two baryonic currents was pioneered in [15]. Subsequently, a different baryonic current was considered in [16–19]. However, this latter version implies that the correlator receives no contribution from the lowest order chiral symmetry breaking operators. We shall use here the proton interpolating current of [15]

$$\eta_N(x) = \varepsilon^{abc} [(u^a)^T(x) C \gamma_\mu u^b(x)] \gamma^\mu \gamma_5 d^c(x), \quad (2)$$

where C is the charge conjugation matrix given by $C = i\gamma_0\gamma_2$. For the neutron case one exchanges the quark flavors, i.e. $u \leftrightarrow d$. In the hadronic sector $\eta(x)$ is defined as

$$\langle 0 | \eta_N(x) | N(p, s) \rangle = \lambda_N u(p, s) e^{ip \cdot x}, \quad (3)$$

with λ_N , the current-nucleon coupling, a phenomenological parameter *a priori* unknown, and $u(p, s)$ is the nucleon spinor. The interpolating function can then be expressed in terms of the nucleon field as $\eta_N(x) = \lambda_N \Psi_N(x)$, and the two-point function is

$$\Pi(q) = i \int d^4x e^{iqx} \langle 0 | T \eta(x) \bar{\eta}(0) | 0 \rangle. \quad (4)$$

In the vacuum, this correlation function involves two independent structures

$$\Pi(q) = \not{q} \Pi_1(q^2) + \Pi_2(q^2). \quad (5)$$

This correlator obeys the Operator Product Expansion (OPE) in the QCD sector. This includes a perturbative contribution associated to a two-loop Feynman diagram, in absence of radiative corrections, as well as a power series of non-perturbative condensates, led by the chiral-quark and the gluon condensates.

In the chiral limit, neglecting radiative corrections, the structures Π_1 and Π_2 in Eq. (5) of the correlator in the QCD sector are [15, 20–22]

$$\begin{aligned} \Pi_1(s) = & -\frac{1}{64\pi^4} s^2 \ln(-s/\nu^2) - \frac{1}{32\pi^3} \langle \alpha_s G^2 \rangle \ln(-s/\nu^2) \\ & - \frac{2}{3} \frac{\langle \bar{q}q\bar{q}q \rangle}{s} + C_8 \frac{\langle \mathcal{O}_8 \rangle}{s^2} + C_{10} \frac{\langle \mathcal{O}_{10} \rangle}{s^3} + \dots, \end{aligned} \quad (6)$$

$$\begin{aligned} \Pi_2(s) = & \frac{1}{4\pi^2} \langle \bar{q}q \rangle s \ln(-s/\nu^2) - \frac{1}{12\pi} \frac{\langle \alpha_s G^2 \bar{q}q \rangle}{s} \\ & + C'_9 \frac{\langle \mathcal{O}_9 \rangle}{s^2} + C'_{11} \frac{\langle \mathcal{O}_{11} \rangle}{s^3} + \dots, \end{aligned} \quad (8)$$

where ν is the dimensional regularization scale, and the correlator components in the hadronic sector are

$$\Pi_1(s) = \frac{-\lambda_N^2}{s - m_N^2}, \quad \Pi_2(s) = \frac{-\lambda_N^2 m_N}{s - m_N^2}. \quad (9)$$

Integrating the two components of the correlator in Eq. (1), and using the FESR kernel $K = 1$ there follow two equations relating the hadronic to the QCD sector

$$\lambda_N^2 = \frac{s_0^3}{192\pi^4} + \frac{s_0}{32\pi^3} \langle \alpha_s G^2 \rangle + \frac{2}{3} \langle \bar{q}q\bar{q}q \rangle, \quad (10)$$

$$\lambda_N^2 m_N = -\frac{s_0^2}{8\pi^2} \langle \bar{q}q \rangle + \frac{1}{12\pi} \langle \alpha_s G^2 \bar{q}q \rangle. \quad (11)$$

Invoking vacuum dominance for the four-quark condensate in Eq. (10) and for the mixed quark and gluon condensate in Eq. (11), a nucleon mass $m_N = 0.94 \text{ GeV}$, the quark condensate $\langle \bar{q}q \rangle = -(0.24 \text{ GeV})^3$, and the *standard* value of the gluon condensate $\langle \alpha_s G^2 \rangle = 0.037 \text{ GeV}^4$, we obtain the values of the current-nucleon coupling $\lambda_N = 0.017 \text{ GeV}^3$ and the hadronic continuum threshold $s_0 = 1.26 \text{ GeV}^2$.

The next step is the evaluation of the FESR in the presence of a constant and uniform magnetic field.

III. MAGNETIC FIELD EFFECTS

A. Propagators

The fermion propagator in the presence of a constant and uniform magnetic field can be written as a power series in qB [8]. Taking into account the anomalous

magnetic moment term $\mathcal{L}_{\text{anom}} = -\frac{1}{2}\kappa\sigma_{\mu\nu}F^{\mu\nu}$ the fermion propagator becomes

$$S(p) = \frac{i(\not{p} + m)}{p^2 - m^2 + i\epsilon} - (qB) \frac{i\sigma_{12}(\not{p}_{\parallel} + m)}{(p^2 - m^2 + i\epsilon)^2} + 2i(qB)^2 \frac{(\not{p}_{\parallel} + m) \left[p_{\perp}^2 - \not{p}_{\perp}(\not{p}_{\parallel} - m) \right]}{(p^2 - m^2 + i\epsilon)^4} - (\kappa B) \frac{i(\not{p} + m)\sigma_{12}(\not{p} + m)}{(p^2 - m^2 + i\epsilon)^2} + \dots, \quad (12)$$

where only relevant terms are considered, and $\sigma_{\mu\nu} \equiv \frac{i}{2}[\gamma_{\mu}, \gamma_{\nu}]$ is the Dirac anti-symmetric tensor.¹ The mass m , charge q and anomalous magnetic moment κ correspond to the respective particles. The charges are $e_p = e$ for protons, $e_n = 0$ for neutrons, $e_u = 2e/3$ for the u -quark and $e_d = -e/3$ for the d -quark. The magnetic anomalous moments are $\kappa_p = 1.79\mu_N$ for protons, $\kappa_n = -1.91\mu_N$ for neutron [23] and $\kappa = 0$ for quarks, with $\mu_N = e/2m_N$ being the nucleon Bohr magneton.

In the case of nucleons, the spatial asymmetry generated by the presence of the external magnetic field will be reflected in the effective nucleon propagator by considering a *transverse velocity* term. The external momentum in the nucleon propagator is written as $p = p_{\parallel} + v_{\perp}p_{\perp}$. The particle velocity is a medium effect, often considered in pionic dynamics [24–26], and smaller than the speed of light. In the case of massless particles v_{\perp} is simply the transverse velocity of the particles [24].

B. Correlators

The most general decomposition of a correlator is given by

$$\Pi = \Pi_S + i\gamma_5\Pi_P + \gamma_{\mu}\Pi_V^{\mu} + \gamma_{\mu}\gamma_5\Pi_A^{\mu} + \sigma_{\mu\nu}\Pi_T^{\mu\nu}, \quad (13)$$

where the sub-indices refer, respectively, to scalar, pseudoscalar, vector, axial-vector and tensor structures. If no topological anomalies are present, then $\Pi_P = 0$. In the vacuum, there are only scalar and vector contributions, with $\Pi_S = \Pi_2$ and $\Pi_V^{\mu} = p^{\mu}\Pi_1$. In the presence of an external uniform-electromagnetic field, the most general combinations of the vector, tensor and axial-vector components involve p_{μ} , $g_{\mu\nu}$, $\epsilon_{\mu\nu\alpha\beta}$ and $F_{\mu\nu}$, on account of the correlator being parity even. For the case of a constant external magnetic field aligned along the third coordinate, the electromagnetic strength tensor can be written as $F_{\mu\nu} = B\epsilon_{\mu\nu}^{\perp}$, where the perpendicular, anti-symmetric tensor is defined as $\epsilon_{\mu\nu}^{\perp} \equiv \epsilon_{0\mu\nu 3}$. The most general decompositions of the vector, axial-vector and tensor structures

in Eq. (13) are given by

$$\Pi_V^{\mu} = p_{\parallel}^{\mu} \Pi_V^{\parallel} + p_{\perp}^{\mu} \Pi_V^{\perp} + \tilde{p}_{\perp}^{\mu} \tilde{\Pi}_V^{\perp}, \quad (14)$$

$$\Pi_A^{\mu} = \tilde{p}_{\parallel}^{\mu} \Pi_A, \quad (15)$$

$$\Pi_T^{\mu\nu} = \epsilon_{\perp}^{\mu\nu} \Pi_T^{\perp} + (p_{\parallel}^{\mu} p_{\perp}^{\nu} - p_{\parallel}^{\nu} p_{\perp}^{\mu}) \Pi_T^{\parallel\perp} + (p_{\parallel}^{\mu} \tilde{p}_{\perp}^{\nu} - p_{\parallel}^{\nu} \tilde{p}_{\perp}^{\mu}) \tilde{\Pi}_T^{\parallel\perp}, \quad (16)$$

where $\tilde{p}_{\perp}^{\mu} \equiv \epsilon_{\perp}^{\mu\alpha} p_{\alpha}$, $\tilde{p}_{\parallel}^{\mu} \equiv \epsilon_{\parallel}^{\mu\alpha} p_{\alpha}$, with the parallel anti-symmetric tensor defined as $\epsilon_{\parallel}^{\mu\nu} \equiv \frac{1}{2}\epsilon^{\mu\nu\alpha\beta}\epsilon_{\alpha\beta}^{\perp} = \epsilon^{\mu 12\nu}$.

In this work we consider the structures Π_S , Π_V^{\parallel} , Π_V^{\perp} and Π_T^{\perp} , in order to compute the FESR.

Usually in the literature the structure decomposition of the correlator is expressed in terms of combinations of external momentum and Dirac matrices [10, 11], which are related to the above structures by

$$F_{\mu\nu}(\not{p}\sigma^{\mu\nu} + \sigma^{\mu\nu}\not{p}) = 4B\gamma_{\mu}\gamma_5\tilde{p}_{\parallel}^{\mu}, \quad (17)$$

$$iF_{\mu\nu}(p^{\mu}\gamma^{\nu} - p^{\nu}\gamma^{\mu})\not{p} = B\sigma_{\mu\nu}(\tilde{p}_{\perp}^{\mu}p_{\parallel}^{\nu} - \tilde{p}_{\perp}^{\nu}p_{\parallel}^{\mu} + \epsilon_{\perp}^{\mu\nu}p_{\perp}^2), \quad (18)$$

which is the axial-vector function Π_A in Eq. (17), and a combination of tensor components $\tilde{\Pi}_T^{\parallel\perp}$ and Π_T^{\perp} in Eq. (18).

C. QCD contour integrals

The advantage of FESR lies on the natural truncation of the non-perturbative OPE series when integrating around the circle in Eq. (1). To visualize this truncation in the presence of external magnetic fields we denote by Π_n the correlator term of order B^n . Then, one has $\Pi_n(s) \sim \frac{\partial^n}{\partial s^n} \Pi_0(s)$. This is easily understood in the chiral limit [12] as the only scales available are s and eB , and the corrections to the vacuum correlator will be of order $(eB/s)^n$. However, there are infrared divergences, which can be handled by including quarks masses. In fact, quarks acquire magnetic masses even in the chiral limit [2, 13].

Considering non-logarithmic contributions, the general structure of a Feynman diagram will be $\Pi(s) \sim \int_{x_i} f(x_i)/[s - \mathcal{M}^2]^n$, where f is some analytic function, n is any integer number, and the integral in terms of Feynman parameters x_i is defined as $\int_{x_i} = \int_0^1 dx_1 \dots dx_k \delta(x_1 + \dots + x_k - 1)$. The mass term, if one considers equal quark masses, is defined as $\mathcal{M}^2 \equiv m_q^2 \left(\frac{1}{x_1} + \dots + \frac{1}{x_k} \right)$. Integrating around the circle of radius s_0 before integrating in the Feynman parameters, one obtains

$$\oint_{s_0} \frac{ds}{2\pi i} s^{N-1} \left[\int_{x_i} \frac{f(x_i)}{[s - \mathcal{M}^2]^n} \right] = \theta_{N-n} \left(\frac{N-1}{n-1} \right) \int_{x_i} \theta(s_0 - \mathcal{M}^2) f(x_i) (\mathcal{M}^2)^{N-n}, \quad (19)$$

¹ Notice that in the literature $\sigma_{\mu\nu}$ is often defined with the opposite sign. This will produce a change in the sign of the condensates $\langle \bar{q}\sigma_{12}q \rangle$.

where the usual step-function is denoted as $\theta(\xi)$, and we define a discrete theta function $\theta_j = 1$ for $j \geq 0$ and $\theta_j = 0$ for $j < 0$. Therefore, the magnetic field powers that participate are limited by the powers of s in the FESR kernel.

The other kind of integrals contain logarithms. Hence, we first integrate around the contour obtaining

$$\oint_{s_0} \frac{ds}{2\pi i} s^{N-1} \left[\int_{x_i} f(x_i) s^n \ln(-s + \mathcal{M}^2) \right] = \frac{1}{N+n} \int_{x_i} \theta(s_0 - \mathcal{M}^2) f(x_i) [s_0^{N+n} - (\mathcal{M}^2)^{N+n}], \quad (20)$$

valid of course for $N + n > 0$.

This is a very useful technique to handle infrared divergences without the need for integrating the Feynman parameters in the full correlator. Once we integrated along the contour, the Heaviside function $\theta(s_0 - \mathcal{M}^2)$ will provide limits of integration to the Feynman parameters. Hence, an expansion in terms of m_q^2/s_0 can be performed to the lowest order leading to logarithmic corrections. These logarithmic contributions are strictly magnetic, thus vanishing for $B = 0$. More details are given in Appendix B.

From the above magnetic power counting, and for sum rules with kernel $K = 1$, it follows that the perturbative part in Eq. (10), and the dimension $d = 3$ condensate contribution in Eq. (11), will have direct magnetic contributions.

It is important to mention that although there is no contribution of dimension-five operators in vacuum, there will be such contributions in a magnetic field. For instance, this happens in the analysis of [10] involving the axial-vector and the tensor structures in Eq. (13). However, they are expected to be negligible for the the magnetic field strengths consider here.

IV. RESULTS

The magnetic FESR involving Π_V^\parallel , Π_V^\perp , Π_S and Π_T^\perp , in the frame $p_\perp = 0$, are as follows:

$$\begin{aligned} \lambda_p^2 = & \frac{s_p^3}{192\pi^4} + \frac{s_p}{32\pi^3} \langle \alpha_s G^2 \rangle + \frac{2}{3} \langle \bar{u}u \rangle^2 + \frac{s_p}{2\pi^4} e_u e_d B^2 \\ & + \frac{s_p}{6\pi^4} (e_u B)^2 [\ln(s_p/8m_q^2) - 1] \\ & + \frac{s_p}{96\pi^4} (e_d B)^2 [8 \ln(s_p/8m_q^2) - 9], \end{aligned} \quad (21)$$

$$\begin{aligned} \lambda_p^2 v_p = & \frac{s_p^3}{192\pi^4} + \frac{s_p}{32\pi^3} \langle \alpha_s G^2 \rangle + \frac{2}{3} \langle \bar{u}u \rangle^2 + \frac{s_p}{4\pi^4} e_u e_d B^2 \\ & - \frac{s_p}{6\pi^4} (e_u B)^2 [\ln(s_p/8m_q^2) - 1] \\ & - \frac{s_p}{96\pi^4} (e_d B)^2 [8 \ln(s_p/8m_q^2) - 9], \end{aligned} \quad (22)$$

$$\begin{aligned} \lambda_p^2 m_p = & -\frac{s_p^2}{8\pi^2} \langle \bar{d}d \rangle + \frac{1}{12\pi} \langle \alpha_s G^2 \rangle \langle \bar{d}d \rangle + \frac{s_p}{2\pi^2} e_u B \langle \bar{d}\sigma_{12}d \rangle \\ & + \frac{4}{3\pi^2} (e_u B)^2 [\ln(s_p/m_q^2) - 1] \langle \bar{d}d \rangle, \end{aligned} \quad (23)$$

$$-\lambda_p^2 \frac{\kappa_p B}{2} = \frac{s_p^2}{48\pi^2} \langle \bar{d}\sigma_{12}d \rangle + \frac{e_u B s_p}{24\pi^2} \langle \bar{d}d \rangle, \quad (24)$$

respectively, where s_p is the proton continuum threshold, λ_p is the current-proton coupling, v_p is the proton transverse velocity and κ_p the proton anomalous magnetic moment.

The FESR for the neutron correlator are the same as above, except for the change in flavor $d \leftrightarrow u$ and $p \leftrightarrow n$. Details of the derivation of the above results are given in Appendix A.

The only new entirely magnetic condensate is the spin polarization one $\langle \bar{q}\sigma_{12}q \rangle$, often referred to as the anomalous magnetic moment condensate. From Eq. (24) it is easy to obtain the quark susceptibility at zero magnetic field, defined as $\chi_q = \langle \bar{q}\sigma_{12}q \rangle / e_q B \langle \bar{q}q \rangle$. At $B = 0$, Eq. (24) gives $\chi_d(0) = -5.50 \text{ GeV}^{-2}$ from proton FESR, while using neutron FESR we find $\chi_d(0) = -3.83 \text{ GeV}^{-2}$. These results are in a good agreement with expectations (see [4] for a literature review on χ_q). The main difference with other determinations is that we do not assume flavor independence. Averaging these two results give $\bar{\chi}_q(0) = -4.67 \text{ GeV}^{-2}$.

A. Inputs

The first input is the quark condensate as a function of an external magnetic field, as obtained in [27], fitted with a Padé approximant. Next, the gluon condensate determined in [2, 3] shows a minor dependence on the magnetic field, so it is assumed constant. Next, the (average) light quark mass in vacuum, following from the Gell-Mann-Oakes-Renner relation, is $m_q(0) = 6.05 \text{ MeV}$, at a scale of 1 GeV . The running values from logarithmic terms have negligible importance in the presence of magnetic fields. Finally, for the third input we consider two scenarios. The first one is to take as input the nucleon mass in order to obtain the condensates $\langle \bar{q}\sigma_{12}q \rangle$. The second possibility is to consider a constant magnetic susceptibility of the quark condensate in order to obtain the nucleon mass.

For the nucleon mass at finite magnetic field there are different behaviors in the literature. Effective models such as the Walecka model, or the linear sigma model or other quark-hadron models, give either increasing masses with increasing magnetic field [6, 8], or no significant variations [5]. Other models, assuming hadron masses as the sum of constituent quark masses, lead to a decreasing nucleon mass [7, 9]. Given that all these different evolutions do no change drastically the final results we keep the nucleon mass constant.

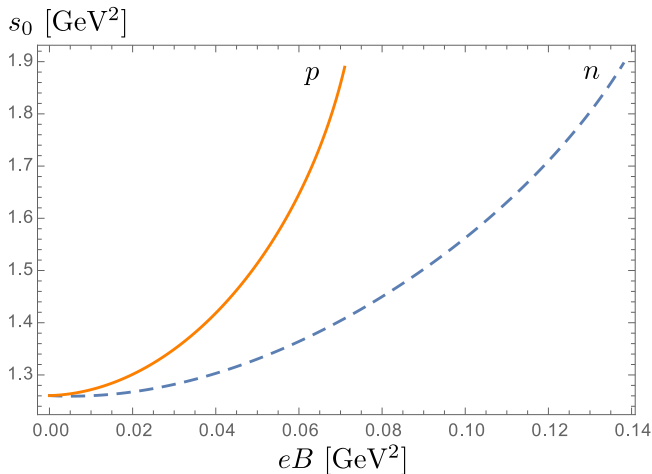


FIG. 1. Continuum hadronic thresholds s_0 as a function of the magnetic field for the proton (solid line) and the neutron correlator (dashed line).

In the case of a constant magnetic susceptibility, one can obtain the magnetic dependence of the nucleon mass for weak magnetic fields.

B. Numerical results

We proceed to solve the set of four equations obtained from the FESR, Eqs. (21)-(24), considering first a constant nucleon mass.

Figure 1 shows the continuum hadronic threshold, $s_0(eB)$ for the nucleon correlators, i.e. for proton and neutron. The upper value of s_0 is chosen below the production threshold of the nucleon resonance $N^*(1440)$, which is not part of this analysis. This truncation is a standard, and convenient procedure in QCD FESR applications. Since the pole mass of the $N^*(1440)$ is about 1.37 GeV [28], then we consider $eB < 0.07 \text{ GeV}^2$ for the proton correlator, and $eB < 0.14 \text{ GeV}^2$ for the nucleon case.

The magnetic behavior of the current-nucleon coupling λ_N , is shown in Fig. 2 for the proton and neutron. We can see that the increasement in the current-nucleon couplings is definitely non negligible, and the change can be larger than 50% of their initial values. The correlator of two nucleonic currents at finite temperature has been explored in [29]. On the contrary with the magnetic field effects, the temperature dependent coupling $\lambda_N(T)$ of the nucleon to the interpolating current turns out to be a monotonically decreasing function, vanishing at T_c .

In Fig. 3, we observe the change of the transverse velocity v_\perp for protons and neutrons, when the magnetic field varies. Both cases have a decreasing behavior and they are always less than the speed of light as it is expected.

In the QCD sector, we determinate the magnetic behavior of the spin polarization condensate $\langle \bar{q}\sigma_{12}q \rangle$, and it is shown in Fig. 4. The up and down quarks exhibit

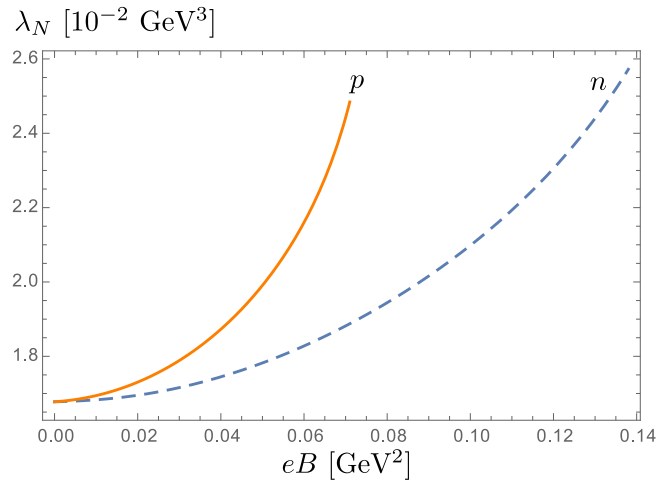


FIG. 2. Current-nucleon coupling for the proton (solid line) and the neutron (dashed line) as a function of the magnetic field strength.

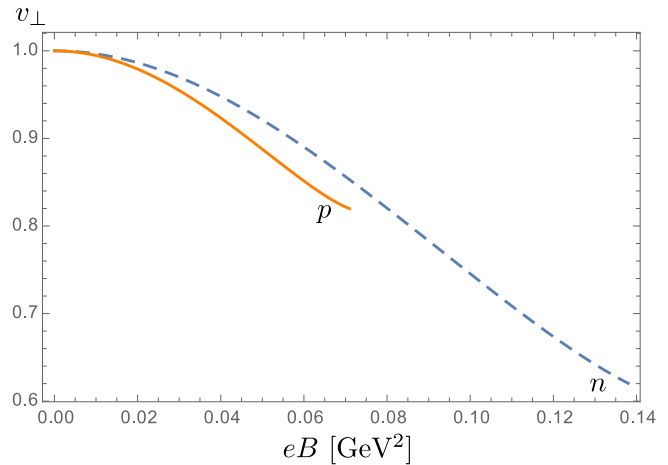


FIG. 3. Transverse velocity as a function of the magnetic field strength. Solid line for proton and dashed line for neutron.

opposite behavior. This is to be expected since they have a different electric charge. The behavior of our result is in agreement with results found in the literature [4, 30].

The magnetic susceptibility for u and d quarks is essentially constant as can be appreciated in Fig. 5 for almost the whole range of values of the magnetic field strength valid in this approach. This means that one can consider a constant magnetic susceptibility as a good approach for low magnetic field. The deflection depends on the inputs. However if we consider a constant magnetic field dependent nucleon mass, the behavior of the magnetic susceptibility does not have a significant change, remaining almost constant for lower values of the magnetic field. This leads us to speculate about what kind of information can be obtained considering a constant magnetic susceptibility, because in this case we have an extra input.

If we now consider the condensates $\langle \bar{q}\sigma_{12}q \rangle \approx e_q B \chi_q(0) \langle \bar{q}q \rangle$ for a given value of the magnetic suscep-

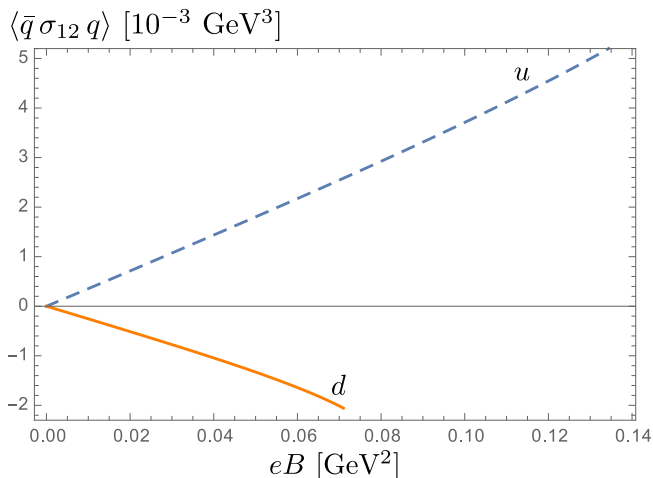


FIG. 4. Magnetic behavior of the spin polarization condensate (also known as anomalous magnetic moment condensate) $\langle \bar{q} \sigma_{1,2} q \rangle$ as a function of the magnetic field. Shown are up-quark (solid line) and down-quark (dashed line) terms.

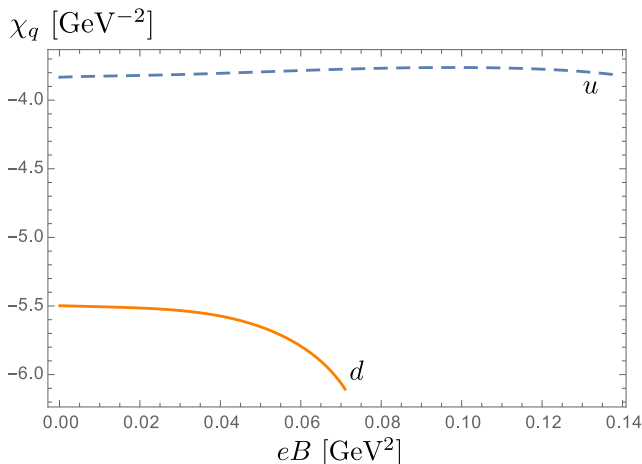


FIG. 5. Magnetic susceptibility of the quark condensate for the down-quark (solid line) and the up-quark (dashed line) as a function of the magnetic field strength.

tibility, we can reduce the number of inputs, and therefore obtain the evolution of nucleon masses at low B . Using the values obtained at $B = 0$ from Fig. 5, i.e. $\chi_d(0) = -5.50 \text{ GeV}^{-2}$ and $\chi_u(0) = -3.83 \text{ GeV}^{-2}$, the resulting nucleon masses are shown in Fig. 6. The maximum values of the magnetic field are obtained by imposing the variation in magnetic susceptibility in Fig. 5 to be less than 0.05 GeV^2 .

The behavior of the nucleon masses agrees with that obtained from lattice QCD results [9] leading to an increasing proton mass and a decreasing neutron mass at low B . The increase of the proton mass agrees with results obtained in [8] from considering the anomalous nucleon magnetic moment.

It is worth mentioning that for the proton case it is not possible to extend the numerical evaluation for

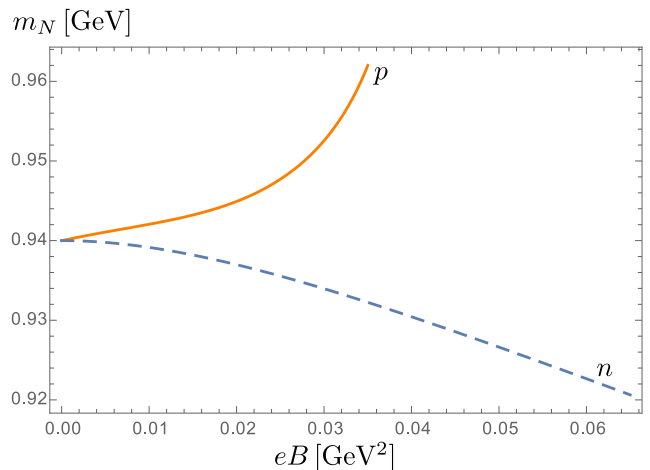


FIG. 6. Proton and neutron masses as a function of the magnetic field strength.

$eB > 0.04 \text{ GeV}^2$, thus highlighting the importance of magnetic effects for the full $\langle \bar{q} \sigma_{12} q \rangle$ condensate. On the other hand, for $eB > 0.12 \text{ GeV}^2$ the neutron mass exhibits an inflection in the curve and starts to grow with the magnetic field. However at this point, the results are unreliable.

The magnetic behavior of the nucleon mass is quite different from that at finite temperature [29] where it remains approximately constant in a wide range of temperature, increasing sharply near the critical deconfinement temperature T_c .

V. CONCLUSIONS

Different nucleon parameters were calculated using FESR for nucleon-nucleon correlators in the presence of an external uniform magnetic field. The evolution of the quark condensates, as function of the magnetic field and the nucleon masses, was considered as an input. The magnetic evolution of the quark condensates is one of the main and direct contributions for the magnetic evolution of the other parameters, in opposition to the case of magnetic evolution of nucleon masses which produces a minimal impact.

The hadronic continuum threshold which delimits the quark-hadron duality was calculated for protons and neutrons obtaining different growing values. The maximum values calculated must be smaller than the mass pole of next nucleon resonances in order to avoid the incorporation of them in the spectral function. This limit provides us with a maximum magnetic field allowed in our approach of $eB < 0.07 \text{ GeV}^2 \approx 3.6 m_\pi^2$ for the proton channel and $eB < 0.14 \text{ GeV}^2 \approx 7 m_\pi^2$ for the neutron channel.

The quantities that can be obtained are the current-nucleon couplings λ_N , which grow with the magnetic field, signaling a stronger confinement of quarks inside

nucleons and can increase in more than 50%. The transverse velocity v_\perp which decreases with the magnetic field as it is expected being smaller than the speed of light. The magnetic moment condensates $\langle \bar{q}\sigma_{12}q \rangle$ is another quantity we have calculated, being in good agreement with the expected behavior from other models. From this quantity, the magnetic susceptibility of the quark condensate χ_q can be obtained, with the interesting behavior that it is almost constant for most of the allowed range of values of the magnetic field intensity. The main difference with many other works is that we have not considered the same magnetic susceptibility for the two light flavors, and in fact the result show they are different.

In particular, the magnetic susceptibility at $B = 0$ can be compared with many other works and it is in good agreement with the range of values of other results. Since $\chi_q(0)$ can be calculated independently of the other sum rules equations, it is possible to obtain the nucleon masses for low magnetic field by keeping $\chi_q(0)$ as an input, valid for low values of the magnetic field. As a result we obtain a behavior that coincides with lattice results, namely that proton mass increases and neutron mass decreases. The increasing proton mass numerically coincides with an analysis in the frame of Walecka model when nucleon anomalous magnetic moment is included.

The increasing of the hadronic threshold and current-nucleon couplings was expected because of previous works, although every channel in principle behaves independently, but it is an insight of stronger confinement. The different behavior of the nucleon masses represents an interesting scenario. Although it is valid for a lower magnetic field, we are talking about $eB < 1.8m_\pi^2$ for protons and $eB < 3.6m_\pi^2$, it is strong enough for magnetic field in magnetars. This is an interesting scenario, worthwhile to be explored including baryonic density effects.

ACKNOWLEDGEMENTS

The authors acknowledge support from FONDECYT (Chile) under grants 1190192, 1170107 and 1200483. M.L. acknowledges support from Conicyt/PIA/Basal (Chile) under grant FB0821. L. A. H. acknowledges support from a PAPIIT-DGAPA-UNAM fellowship. C.A.D. was supported in part by the Alexander von Humboldt Foundation (Germany), and the University of Cape Town.

Appendix A: Magnetic correlators

This appendix deals with current correlator terms in the presence of an external magnetic field. *Magnetic field insertion* is the name given to the individual propagators from Eq. (12). They are expressed in powers of $B/(p^2 - m^2)$, and diagrammatically correspond to a single, double, or higher number of external lines, depending on the power of B . Figure 7 shows all diagrams with

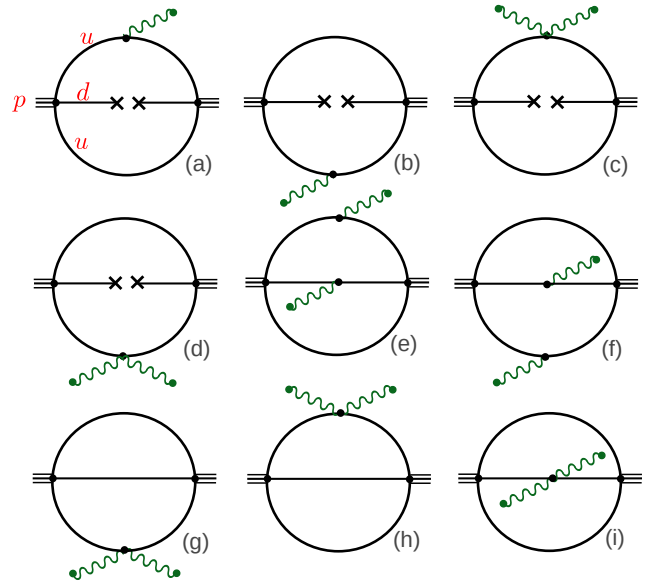


FIG. 7. Non-vanishing Feynman diagrams with magnetic insertions used in this work. The diagrams correspond to proton-proton propagator. The case of neutron correlator is the same but interchanging $u \leftrightarrow d$ lines.

magnetic field insertions, including propagators. The relevant diagrams are the one-loop ones, corresponding to the dimension-3 contribution in the OPE (quark condensate), i.e. diagrams (a) to (d). The perturbative ones in the OPE are two-loop diagrams (e) to (i). Notice that we do not include two-loop diagrams with one magnetic field insertion. This is because they only contribute to the axial component of the structure decomposition in Eq. (13). This is not considered here. Also notice the vanishing of one-loop and two-loop diagrams with one magnetic insertion, with the top u -propagator and one magnetic insertion from the bottom u -propagator. Finally, we only consider contributions to the correlators Π_S , Π_V and Π_T from Eq. (13), as well as Π_V^\parallel and Π_V^\perp from Eq. (14), and Π_T^\perp from Eq. (16). Results are expressed in the frame $p_\perp^2 = 0$, with $p_\parallel^2 = s$.

1. One-loop diagrams

The correlator corresponding to diagrams involving operators of dimension $d = 3$ is given by

$$\Pi = i \int \frac{d^4 k}{(2\pi)^4} \text{tr}[\gamma_\mu S_u(k) \gamma_\nu C S_u(q-k) C] \times \gamma^\mu [\langle \bar{d}d \rangle + \sigma_{12} \langle \bar{d}\sigma_{12}d \rangle] \gamma^\nu. \quad (\text{A1})$$

This correlator corresponds to the proton diagrams (a) to (d) in Fig 7. Notice that the only condensate is the one in the d -line. This is because when cutting the top or bottom u -lines the correlator vanishes after performing the trace.

The first new contribution is that of the spin polarization condensate, also entering the diagram without magnetic field insertion. It contributes to the tensor part in the structure decomposition in Eq. (16),

$$\Pi_{T(0)}^\perp = -\frac{1}{24\pi^2} s \ln(-s/\nu^2) \langle \bar{d} \sigma_{12} d \rangle, \quad (\text{A2})$$

where the subscript (0) indicates that it is of order B^0 . This contribution does not involve magnetic insertions, with magnetic effects implicit in the spin polarization condensate.

Diagrams (a)+(b) give a contribution to a scalar and to a tensor component

$$\Pi_{S(a+b)} = -\frac{e_u B}{2\pi^2} \ln(-s/\nu^2) \langle \bar{d} \sigma_{12} d \rangle, \quad (\text{A3})$$

$$\Pi_{T(a+b)}^\perp = \frac{e_u B}{4\pi^2} \ln(-s/\nu^2) \langle \bar{d} d \rangle. \quad (\text{A4})$$

Diagrams (c)+(d) generate a contribution to a tensor component, not considered here, and a contribution to the scalar component which gives

$$\Pi_{S(c+d)} = -\frac{4}{\pi^2} (e_u B)^2 \int_x \frac{1-x}{3x} \frac{1}{p^2 - \mathcal{M}_1^2} \langle \bar{d} d \rangle, \quad (\text{A5})$$

with $\mathcal{M}_1 = m_q^2/x(1-x)$. This last equation vanishes in the chiral limit. Hence, it is not necessary to keep the quark mass in the denominator to regularize it. Details of the integration in Feynman parameters is given in Appendix B.

2. Two-loop diagrams

The perturbative correlator corresponding to two-loop diagrams is

$$\Pi = 12i \int \frac{d^4 k}{(2\pi)^4} \frac{d^4 p}{(2\pi)^4} \text{tr}[\gamma_\mu S_u(k) \gamma_\nu C S_u(p) C] \times \gamma^\mu S_d(q-k-p) \gamma^\nu. \quad (\text{A6})$$

Diagrams (e) and (f), as well as diagrams (g) and (h) give the same result. All diagrams from (e) to (i) contribute only to the vector component of the correlator.

The parallel vector components are

$$\Pi_{V(e+f)}^\parallel = -\frac{e_u e_d B^2}{2\pi^4} \ln(-s), \quad (\text{A7})$$

$$\Pi_{V(g+h)}^\parallel = -\frac{(e_u B)^2}{\pi^4} \int_0^1 dx dy \ln(-s + \mathcal{M}_2^2) \times \frac{xy^4(1-y)z}{(xy + yz + zx)^5}, \quad (\text{A8})$$

$$\Pi_{V(i)}^\parallel = -\frac{(e_d B)^2}{4\pi^4} \int_0^1 dx dy \ln(-s + \mathcal{M}_2^2) \times \frac{2xy^4(1-y)z - x^2 y^3 z^2}{(xy + yz + zw)^5}, \quad (\text{A9})$$

with $\mathcal{M}_2^2 = m_q^2(\frac{1}{x} + \frac{1}{y} + \frac{1}{z})$ and $z = 1 - x - y$.

The perpendicular vector components are

$$\Pi_{V(e+f)}^\perp = \frac{1}{2} \Pi_{V(e+f)}^\parallel, \quad (\text{A10})$$

$$\Pi_{V(g+h)}^\perp = -\Pi_{V(g+h)}^\parallel, \quad (\text{A11})$$

$$\Pi_{V(i)}^\perp = -\Pi_{V(i)}^\parallel. \quad (\text{A12})$$

The quark mass entering the logarithms of diagrams (g), (h), and (i) is kept finite in order to regularize infrared divergences.

Appendix B: Feynman parameters

Integrating the QCD contributions on the contour in the s -plane leads to integrals involving Feynman parameters, as described in Eqs. (19) and (20). The quark mass regularizes infrared divergences entering diagrams Fig. 7 (c), (d), (g) and (h), as described next.

1. One-loop diagrams

Diagrams with a quark condensate are one-loop. From Eq. (19) they are written as

$$\oint_{s_0} \frac{ds}{2\pi i} \Pi_{1\text{-loop}} = \int_0^1 dx dy \delta(x+y-1) \theta(s_0 - \mathcal{M}_1^2) f(x, y), \quad (\text{B1})$$

with $\mathcal{M}_1^2 = m_q^2(\frac{1}{x} + \frac{1}{y})$, and $f(x, y)$ an analytic function. Integrating in y , with the restrictions from the δ - and the θ -function, gives

$$\oint_{s_0} \frac{ds}{2\pi i} \Pi_{1\text{-loop}} = \theta(s_0 - 4m_q^2) \int_{x_-}^{x_+} dx f(x, 1-x), \quad (\text{B2})$$

where the integration limits for equal quark masses are $x_\pm = \frac{1}{2} [1 \pm \sqrt{1 - 4m_q^2/s_0}]$. For $m_q \rightarrow 0$ one recovers the usual limits $x_- = 0$ and $x_+ = 1$.

The specific one-loop diagrams needed for this regularization are (c) and (d) in Fig. 7. Integrating Eq. (A5) on the contour in s , and then expanding in $m_q/s_0 \rightarrow 0$ up to first order gives

$$\oint_{s_0} \frac{ds}{2\pi i} \Pi_{S(c+d)} = -\frac{4}{3\pi^2} (e_u B)^2 [\ln(s_p/m_q^2) - 1] \langle \bar{d} d \rangle. \quad (\text{B3})$$

2. Two-loop diagrams

The perturbative diagrams at the two-loop level involve logarithmic terms and can be written as

$$\oint_{s_0} \frac{ds}{2\pi i} \Pi_{2\text{-loop}} = \int_0^1 dx dy dz \delta(x+y+z-1) \times \theta(s_0 - \mathcal{M}_2^2) f(x, y, z) [s_0 - \mathcal{M}_2^2], \quad (\text{B4})$$

with $\mathcal{M}_2^2 = m_q^2(\frac{1}{x} + \frac{1}{y} + \frac{1}{z})$ and $f(x, y, z)$ an analytic function. Integrating in z , and considering the restrictions from the δ - and θ -functions, gives

$$\oint_{s_0} \frac{ds}{2\pi i} \Pi_{2\text{-loop}} = \theta(s_0 - 9m_q^2) \times \int_{x_-}^{x_+} dx \int_{y_-}^{y_+} dy f(x, y, z)[s_0 - \mathcal{M}_2^2], \quad (\text{B5})$$

with $z = 1 - x - y$ and

$$x_{\pm} = \frac{1}{2} \left[1 - \frac{3m^2}{s_0} \pm \sqrt{\left(1 - \frac{3m^2}{s_0}\right)^2 - \frac{4m^2}{s_0}} \right], \quad (\text{B6})$$

$$y_{\pm} = \frac{1}{2} \left[1 - x \pm \sqrt{(1-x)^2 - \frac{4m^2 x(1-x)}{s_0 x - m^2}} \right]. \quad (\text{B7})$$

In the limit $m_q \rightarrow 0$ one recovers the usual limits $x_- = 0$, $x_+ = 1$, $y_- = 0$ and $y_+ = 1 - x$.

There are four non-trivial integrals involved here, as can be seen from Eqs. (A8) and (A9). All these integrals can be evaluated analytically when integrating in the variable y , but not in x which will require some fitting. Starting with the last term in Eq. (A9), in the limit $m_q \rightarrow 0$, which becomes

$$\int_{x_-}^{x_+} dx \int_{y_-}^{y_+} \frac{x^2 y^3 z^2}{(xy + yz + zx)^5} [s_p - \mathcal{M}_2^2] = \frac{s_p}{12}. \quad (\text{B8})$$

The term in this integral proportional to s_p can be obtained directly in the chiral limit. The term proportional to \mathcal{M}_2^2 is evaluated numerically, but it vanishes in the limit $m_q \rightarrow 0$. Next term is the one that enters in both equations (A8) and (A9). In the limit $m_q \rightarrow 0$ it becomes

$$\int_{x_-}^{x_+} dx \int_{y_-}^{y_+} \frac{xy^4(1-y)z}{(xy + yz + zx)^5} [s_p - \mathcal{M}_2^2] \approx \frac{s_p}{6} [\ln(s_p/8m_q^2) - 1], \quad (\text{B9})$$

where it corresponds to a fit of the result expressed as an integral in x , as a function of m_q^2/s_p . From these considerations, the contour integral of Eqs. (A8) and (A9) leads to

$$\oint_{s_p} \frac{ds}{2\pi i} \Pi_{V(g+h)}^{\parallel} = -\frac{(e_u B)^2}{12\pi^4} s_p [\ln(s_p/8m_q^2) - 1], \quad (\text{B10})$$

$$\oint_{s_p} \frac{ds}{2\pi i} \Pi_{V(i)}^{\parallel} = -\frac{(e_d B)^2}{96\pi^4} s_p [8 \ln(s_p/8m_q^2) - 9]. \quad (\text{B11})$$

-
- [1] D. Kharzeev, K. Landsteiner, A. Schmitt, and H. Yee, eds., *Strongly Interacting Matter in Magnetic Fields* (Springer, 2013).
 - [2] C. Dominguez, M. Loewe, and C. Villavicencio, *Phys. Rev. D* **98**, 034015 (2018), arXiv:1806.10088 [hep-ph].
 - [3] M. D'Elia, E. Meggiolaro, M. Mesiti, and F. Negro, *Phys. Rev. D* **93**, 054017 (2016), arXiv:1510.07012 [hep-lat].
 - [4] M. Frasca and M. Ruggieri, *Phys. Rev. D* **83**, 094024 (2011), arXiv:1103.1194 [hep-ph].
 - [5] P. Yue and H. Shen, *Phys. Rev. C* **77**, 045804 (2008), arXiv:0804.3027 [nucl-th].
 - [6] A. Haber, F. Preis, and A. Schmitt, *Phys. Rev. D* **90**, 125036 (2014), arXiv:1409.0425 [nucl-th].
 - [7] H. Taya, *Phys. Rev. D* **92**, 014038 (2015), arXiv:1412.6877 [hep-ph].
 - [8] A. Mukherjee, S. Ghosh, M. Mandal, S. Sarkar, and P. Roy, *Phys. Rev. D* **98**, 056024 (2018), arXiv:1809.07028 [hep-ph].
 - [9] G. Endrödi and G. Markó, *JHEP* **08**, 036 (2019), arXiv:1905.02103 [hep-lat].
 - [10] B. Ioffe and A. V. Smilga, *Nucl. Phys. B* **232**, 109 (1984).
 - [11] L. Wang and F. X. Lee, *Phys. Rev. D* **78**, 013003 (2008), arXiv:0804.1779 [hep-ph].
 - [12] A. Ayala, C. Dominguez, L. Hernandez, M. Loewe, J. C. Rojas, and C. Villavicencio, *Phys. Rev. D* **92**, 016006 (2015), arXiv:1504.01308 [hep-ph].
 - [13] C. Villavicencio, C. Dominguez, and M. Loewe, *J. Phys. Conf. Ser.* **1602**, 012027 (2020), arXiv:2007.05642 [hep-ph].
 - [14] C. A. Dominguez, *Quantum Chromodynamics Sum Rules*, SpringerBriefs in Physics (Springer International Publishing, Cham, 2018).
 - [15] B. Ioffe, *Nucl. Phys. B* **188**, 317 (1981), [Erratum: *Nucl. Phys. B* 191, 591–592 (1981)].
 - [16] Y. Chung, H. G. Dosch, M. Kremer, and D. Schall, *Phys. Lett. B* **102**, 175 (1981).
 - [17] Y. Chung, H. G. Dosch, M. Kremer, and D. Schall, *Nucl. Phys. B* **197**, 55 (1982).
 - [18] Y. Chung, H. G. Dosch, M. Kremer, and D. Schall, *Z. Phys. C* **15**, 367 (1982).
 - [19] Y. Chung, H. G. Dosch, M. Kremer, and D. Schall, *Z. Phys. C* **25**, 151 (1984).
 - [20] L. Reinders, H. Rubinstein, and S. Yazaki, *Phys. Rept.* **127**, 1 (1985).
 - [21] V. Sadovnikova, E. Drukarev, and M. Ryskin, *Phys. Rev. D* **72**, 114015 (2005), arXiv:hep-ph/0508240.
 - [22] N. F. Nasrallah and K. Schilcher, *Phys. Rev. C* **89**, 045202 (2014), [Addendum: *Phys. Rev. C* 89, 059904 (2014)], arXiv:1310.6114 [hep-ph].
 - [23] C. Patrignani *et al.* (Particle Data Group), *Chin. Phys. C* **40**, 100001 (2016).
 - [24] K. Kamikado and T. Kanazawa, *JHEP* **03**, 009 (2014), arXiv:1312.3124 [hep-ph].
 - [25] R. D. Pisarski and M. Tytgat, *Phys. Rev. D* **54**, 2989 (1996), arXiv:hep-ph/9604404.
 - [26] D. Son and M. A. Stephanov, *Phys. Rev. D* **61**, 074012 (2000), arXiv:hep-ph/9908052 [hep-ph].

- (2000), [arXiv:hep-ph/9910491](#).
- [27] G. Bali, F. Bruckmann, G. Endrodi, Z. Fodor, S. Katz, and A. Schafer, *Phys. Rev. D* **86**, 071502 (2012), [arXiv:1206.4205 \[hep-lat\]](#).
- [28] M. Tanabashi *et al.* (Particle Data Group), *Phys. Rev. D* **98**, 030001 (2018).
- [29] C. Dominguez and M. Loewe, *Z. Phys. C* **58**, 273 (1993).
- [30] G. S. Bali, G. Endrödi, and S. Piemonte, *JHEP* **07**, 183 (2020), [arXiv:2004.08778 \[hep-lat\]](#).